



Deposited via The University of York.

White Rose Research Online URL for this paper:

<https://eprints.whiterose.ac.uk/id/eprint/165594/>

Version: Accepted Version

---

**Article:**

Bello Garrote, F. L., Sahin, E., Tsunoda, Y. et al. (2020)  $\beta$  decay of  $^{75}\text{Ni}$  and the systematics of the low-lying level structure of neutron-rich odd- $A$  Cu isotopes. *Physical Review C - Nuclear Physics*. 034314. ISSN: 2469-9993

<https://doi.org/10.1103/PhysRevC.102.034314>

---

**Reuse**

Items deposited in White Rose Research Online are protected by copyright, with all rights reserved unless indicated otherwise. They may be downloaded and/or printed for private study, or other acts as permitted by national copyright laws. The publisher or other rights holders may allow further reproduction and re-use of the full text version. This is indicated by the licence information on the White Rose Research Online record for the item.

**Takedown**

If you consider content in White Rose Research Online to be in breach of UK law, please notify us by emailing [eprints@whiterose.ac.uk](mailto:eprints@whiterose.ac.uk) including the URL of the record and the reason for the withdrawal request.

# $\beta$ -decay of $^{75}\text{Ni}$ and the systematics of the low-lying level structure of neutron-rich odd-A Cu isotopes.

F. L. Bello Garrote,<sup>1</sup> E. Sahin,<sup>1</sup> Y. Tsunoda,<sup>2</sup> T. Otsuka,<sup>2,3,4,5</sup> A. G3rger,<sup>1</sup> M. Niikura,<sup>3</sup> S. Nishimura,<sup>6</sup> G. de Angelis,<sup>7</sup> G. Benzoni,<sup>8</sup> A.I. Morales,<sup>9,8,10</sup> V. Modamio,<sup>1</sup> Z. Y. Xu,<sup>3</sup> H. Baba,<sup>6</sup> F. Browne,<sup>6,11</sup> A.M. Bruce,<sup>11</sup> S. Ceruti,<sup>8</sup> F. Crespi,<sup>8</sup> R. Daido,<sup>12</sup> M.-C. Delattre,<sup>13</sup> P. Doornenbal,<sup>6</sup> Zs. Dombradi,<sup>14</sup> Y. Fang,<sup>12</sup> S. Franchoo,<sup>13</sup> G. Gey,<sup>6,15</sup> A. Gottardo,<sup>7</sup> K. Hadyńska-Kleń,<sup>16</sup> T. Isobe,<sup>6</sup> P.R. John,<sup>17</sup> H.S. Jung,<sup>18</sup> I. Kojouharov,<sup>19</sup> T. Kubo,<sup>6</sup> N. Kurz,<sup>19</sup> I. Kuti,<sup>14</sup> Z. Li,<sup>20</sup> G. Lorusso,<sup>6</sup> I. Matea,<sup>13</sup> K. Matsui,<sup>3</sup> D. Mengoni,<sup>17</sup> T. Miyazaki,<sup>3</sup> S. Momiyama,<sup>3</sup> P. Morfouace,<sup>13</sup> D.R. Napoli,<sup>7</sup> F. Naqvi,<sup>21</sup> H. Nishibata,<sup>12</sup> A. Odahara,<sup>12</sup> R. Orlandi,<sup>22,23</sup> Z. Patel,<sup>6,16</sup> S. Rice,<sup>6,16</sup> H. Sakurai,<sup>3,6</sup> H. Schaffner,<sup>19</sup> L. Sinclair,<sup>6,24</sup> P.-A. S3oderstr3m,<sup>6</sup> D. Sohler,<sup>14</sup> I.G. Stefan,<sup>13</sup> T. Sumikama,<sup>25</sup> D. Suzuki,<sup>13</sup> R. Taniuchi,<sup>3</sup> J. Taprogge,<sup>6,26,27</sup> Zs. Vajta,<sup>6,14</sup> J.J. Valiente-Dob3n,<sup>7</sup> H. Watanabe,<sup>28</sup> V. Werner,<sup>21,29</sup> J. Wu,<sup>6,20</sup> A. Yagi,<sup>12</sup> M. Yalcinkaya,<sup>30</sup> R. Yokoyama,<sup>3</sup> and K. Yoshinaga<sup>31</sup>

<sup>1</sup>University of Oslo, Department of Physics, N-0316 Oslo, Norway

<sup>2</sup>Center for Nuclear Study, University of Tokyo, Hongo, Bunkyo-ku, Tokyo 113-0033, Japan

<sup>3</sup>Department of Physics, University of Tokyo, 7-3-1 Hongo, Bunkyo, Tokyo 113-0033, Japan

<sup>4</sup>National Superconducting Cyclotron Laboratory, Michigan State University, East Lansing, Michigan 48824, USA

<sup>5</sup>Instituut voor Kern- en Stralingsfysica, KU Leuven, B-3001 Leuven, Belgium

<sup>6</sup>RIKEN Nishina Center, 2-1 Hirosawa, Wako, Saitama 351-0198, Japan

<sup>7</sup>Istituto Nazionale di Fisica Nucleare, Laboratori Nazionali di Legnaro, I-35020 Legnaro, Italy

<sup>8</sup>Istituto Nazionale di Fisica Nucleare, Sezione di Milano, Via Celoria 16, 20133 Milano, Italy

<sup>9</sup>Dipartimento di Fisica dell'Universit3 degli Studi di Milano, Via Celoria 16, 20133 Milano, Italy

<sup>10</sup>IFIC, CSIC-Universitat de Val3ncia, E-46071 Val3ncia, Spain

<sup>11</sup>School of Computing, Engineering and Mathematics,

University of Brighton, Brighton, BN2 4GJ, UK

<sup>12</sup>Department of Physics, Osaka University, 1-1 Machikaneyama, Toyonaka, Osaka 560-0043, Japan

<sup>13</sup>Institut de Physique Nucleaire (IPN), IN2P3-CNRS,

Universite Paris-Sud 11, F-91406 Orsay Cedex, France

<sup>14</sup>Institute for Nuclear Research of the Hungarian Academy of Sciences, Debrecen H-4001, Hungary

<sup>15</sup>LPSC, Universite Joseph Fourier Grenoble 1, CNRS/IN2P3,

Institut National Polytechnique de Grenoble, F-38026 Grenoble Cedex, France

<sup>16</sup>Department of Physics, University of Surrey, Guildford GU2 7XH, United Kingdom

<sup>17</sup>INFN Sezione di Padova and Dipartimento di Fisica e Astronomia, Universit3 di Padova, Padova, Italy

<sup>18</sup>Department of Physics, University of Notre Dame, Notre Dame, Indiana 46556, USA

<sup>19</sup>GSI Helmholtzzentrum f3r Schwerionenforschung GmbH, 64291 Darmstadt, Germany

<sup>20</sup>Department of Physics, Peking University, Beijing 100871, China

<sup>21</sup>Wright Nuclear Structure Laboratory, Yale University, New Haven, CT 06520-8120, US

<sup>22</sup>Instituut voor Kern- en Stralingsfysica, K.U. Leuven, B-3001 Heverlee, Belgium

<sup>23</sup>Advanced Science Research Center, JAEA, Tokai, Ibaraki 319-1195, Japan

<sup>24</sup>Department of Physics, University of York, Heslington, York YO10 5DD, United Kingdom

<sup>25</sup>Department of Physics, Tohoku University, 6-3 Aramaki-Aoba, Aoba, Sendai 980-8578, Japan

<sup>26</sup>Departamento de Fisica Teorica, Universidad Autonoma de Madrid, E-28049 Madrid, Spain

<sup>27</sup>Instituto de Estructura de la Materia, CSIC, E-28006 Madrid, Spain

<sup>28</sup>International Research Center for Nuclei and Particles in the Cosmos, Beihang University, Beijing 100191, China

<sup>29</sup>Institut f3r Kernphysik, TU Darmstadt, 64289 Darmstadt, Germany

<sup>30</sup>Department of Physics, Faculty of Science, Istanbul University, Vezneciler/Fatih, 34134, Istanbul, Turkey

<sup>31</sup>Department of Physics, Tokyo University of Science, 2641 Yamazaki, Noda, Chiba 278-8510, Japan

(Dated: July 15, 2019)

**Background:** Detailed spectroscopy of neutron-rich odd-A Cu isotopes is of great importance for studying the shell evolution in the region of  $^{78}\text{Ni}$ . While there is experimental information on excited states in  $^{69-73,77,79}\text{Cu}$  isotopes, the information concerning  $^{75}\text{Cu}$  is very limited.

**Purpose:** Experimentally observed single-particle, core-coupling, and proton-hole intruder states in  $^{75}\text{Cu}$ , will complete the systematics of these states in the chain of isotopes.

**Method:** Excited states in  $^{75}\text{Cu}$  were populated in the  $\beta$ -decay of  $^{75}\text{Ni}$  isotopes. The Ni nuclei were produced by the in-flight fission of  $^{238}\text{U}$  projectiles, and were separated, identified, and implanted in a highly segmented Si detector array for the detection of the  $\beta$ -decay electrons. The  $\beta$ -delayed  $\gamma$  rays were detected in a HPGe cluster array. Monte Carlo shell model calculations were performed using the A3DA interaction built on the  $pf_{9/2}d_{5/2}$  model space for both neutrons and protons.

**Results:** A level scheme of  $^{75}\text{Cu}$  was built up to  $\sim 4$  MeV by performing a  $\gamma$ - $\gamma$  coincidence analysis. The excited states below 2 MeV were interpreted based on the systematics of neutron rich odd-A Cu isotopes and the results of the shell model calculations.

**Conclusions:** The evolution of the single-particle, core-coupling, and proton-hole intruder states in the chain of neutron-rich odd-A Cu isotopes is discussed in the present work, in connection with the newly observed level structure of  $^{75}\text{Cu}$ .

## I. INTRODUCTION

The shell structure of exotic nuclei towards the drip-lines is expected to differ from that of stable nuclei. Theoretical predictions and existing experimental data so far indicate that the nuclear shell structure, now recognized as a more local than global concept within the nuclear chart, is not as robust as previously thought [1]; the weakening of the spherical shell gaps has been shown to be closely related to the tensor component of the monopole shell-model Hamiltonian [2, 3]. The region near the doubly-magic nucleus  $^{78}\text{Ni}$ , with its very large neutron-to-proton ratio, is of great interest for shell evolution studies, but continues to be, at the moment, very difficult to investigate experimentally. Here, the systematic study of the excited states of neutron-rich, odd-A Cu isotopes from  $A = 69$  to 79 plays a vital role in understanding the structural changes between the  $N = 40$  sub-shell and  $N = 50$  shell closures. Shell-model calculations find modifications of the proton single-particle energies in the Ni chain with increasing the number of neutrons in the  $\nu 1g_{9/2}$  orbital, leading to the inversion of the  $\pi 2p_{3/2}$  and  $\pi 1f_{5/2}$  orbitals [2–4]. This was confirmed by measuring the inversion of the  $3/2^-$  and  $5/2^-$  states in the neutron-rich odd-A Cu isotopes [5, 6]. After considering the experimentally available information on excited states in  $^{77}\text{Cu}$ , the size of the  $Z = 28$  shell gap was found to be reduced to approximately 5 MeV at  $N = 50$  [7].

Spectroscopic information on the low-lying states in  $^{69-73}\text{Cu}$  has been obtained in  $\beta$ -decay [8], Coulomb excitation [9], and lifetime-measurement experiments [10]. In  $^{69,71}\text{Cu}$ , higher spin states are known from fragmentation [11] and multi-nucleon transfer reactions [12–15]. In  $^{77}\text{Cu}$ , excited states were populated in the  $\beta$ -decay of  $^{77}\text{Ni}$  [7] and in the single proton knock-out of  $^{78}\text{Zn}$  [16]. In  $^{79}\text{Cu}$ , excited states up to  $\sim 4.5$  MeV have been observed for the first time in a proton knockout reaction [17]. In  $^{75}\text{Cu}$ , previous to the present work, only two low-lying isomeric states had been reported from fragmentation reactions [18–20]. The level scheme obtained in the present  $\beta$ -decay study fills the gap in the systematics of the neutron-rich, odd-A Cu isotopes, providing a more complete picture for studying the shell evolution in the region of  $^{78}\text{Ni}$ . In parallel with the present work, results from a proton knockout experiment on  $^{75}\text{Cu}$  and  $^{77}\text{Cu}$  are presented [21], establishing the nature of some of the observed states in these isotopes.

## II. EXPERIMENTAL SETUP

The data presented in this work originates from separate experiments performed during the EURICA campaign [22] at the Radioactive Ion Beam Factory (RIBF) [23] of the RIKEN Nishina Center. A primary beam of  $^{238}\text{U}$  with 345 A MeV energy was delivered by the RIKEN accelerator complex [24] with an average intensity of 10 pnA. Short-lived, neutron-rich nuclides were produced by in-flight fission of the  $^{238}\text{U}$  projectiles on a  $^9\text{Be}$  target with 555 mg/cm<sup>2</sup> thickness. Fragments of interest were selected in the first part of the BigRIPS fragment separator [25] using the  $B\rho$ - $\Delta E$ - $B\rho$  method [26]. These experiments aimed at studying nuclei in the region near  $^{78}\text{Ni}$  and used very similar settings of the BigRIPS separator for the selection of the fragments [27]. The particle identification (PID) was performed using the TOF- $B\rho$ - $\Delta E$  method [28], making use of the beam-line detectors both in the second half of BigRIPS and in the ZeroDegree spectrometer [25]. A PID plot from the experiments can be found in Ref. [29]. The  $^{75}\text{Ni}$  ions were transmitted to the detection system, where their  $\beta$ -decay to  $^{75}\text{Cu}$  and subsequent  $\gamma$  decay was detected.

The secondary beam of radioactive ions was implanted into the wide-range active silicon strip stopper array for beta and ion detection (WAS3ABi) [30], which consisted of a stack of 8 DSSSD detectors located at the last focal point (F11) of the ZeroDegree spectrometer. Each DSSSD had 60 horizontal and 40 vertical strips of 1 mm pitch, respectively, giving a total of 2400 1x1 mm<sup>2</sup> pixels in each detector. The DSSSDs had a thickness of 1 mm and were separated in depth by 0.5 mm. The velocity of the fragments was reduced by an aluminum degrader located in front of WAS3ABi to ensure the implantation of the desired fragments in the center of the stack. A timestamp value was recorded for all the implantation and  $\beta$ -decay events detected in WAS3ABi. The EUROBALL-RIKEN Cluster Array (EURICA) of germanium detectors [22] was surrounding WAS3ABi with the purpose of detecting  $\beta$ -delayed  $\gamma$  rays. The average absolute photo-peak efficiency of the EURICA array during the experiments was  $\sim 6.5\%$  at 1.33 MeV.

## III. DATA ANALYSIS AND EXPERIMENTAL RESULTS

The incoming  $^{75}\text{Ni}$  ions were correlated in time with implantation events and subsequent  $\beta$ -decay electrons detected in WAS3ABi. To correlate the  $\beta$ -decay signals with the implanted  $^{75}\text{Ni}$  ions it was required that they originated from the same DSSSD within a correlation



TABLE I. Energies ( $E_\gamma$ ) and absolute intensities ( $I_\gamma$ ) of the  $\gamma$ -ray transitions assigned to  $^{75}\text{Cu}$ . For those transitions placed in the level scheme of Fig. 5, the initial states ( $E_i$ ) are indicated. Transitions that could not be placed in the level scheme are given in parentheses. The intensities of the 61.8 and 66.2 keV isomeric transitions were corrected for the finite size of the time window that was set for the collection of the  $\gamma$  rays. The intensities are corrected for internal conversion, using conversion coefficients calculated from Ref. [33].

$E_\gamma$ [keV]	$E_i$ [keV] <sup>a</sup>	$I_\gamma$ [%]	$E_\gamma$ [keV] <sup>a</sup>	$E_i$ [keV] <sup>a</sup>	$I_\gamma$ [%]	$E_\gamma$ [keV] <sup>a</sup>	$E_i$ [keV] <sup>a</sup>	$I_\gamma$ [%]	$E_\gamma$ [keV] <sup>a</sup>	$E_i$ [keV] <sup>a</sup>	$I_\gamma$ [%]
61.8	61.8	12.6(38)	734.1 <sup>d</sup>	2414.5	0.81(56)	1236.1	2228.3	2.06(14)	(1866.5)		<0.3
66.2	66.2	10.0(20) <sup>b</sup>	776.2	1726.1	4.99(18)	1261.2	2253.3	0.70(11)	(1874.9)		0.31(11)
		2.99(58) <sup>c</sup>	812.6	3227.1	5.79(20)	(1273.1)		1.04(12)	(2069.4)		<0.3
362.5	2351.6	1.92(17)	826.7	1819.0	5.02(19)	1299.9	2351.6	2.46(14)	2142.8	3135.9	0.50(11)
368.4	2357.4	0.74(13)	842.8 <sup>d</sup>	3194.4	2.12(50)	1322.1	2805.4	2.71(16)	2186.1	3135.9	1.81(16)
425.5	2414.5	0.71(13)	844.3 <sup>d</sup>	2833.3	2.89(47)	1359.4	2351.6	5.24(20)	(2279.4)		<0.3
434.2	2253.3	1.61(15)	868.1	2351.6	2.64(15)	1371.4	3963.9	0.58(14)	(2286.1)		<0.3
453.7	2805.4	1.35(14)	883.6	949.7	15.64(37)	(1392.7)		0.48(9)	(2357.7)		0.77(11)
491.1	1483.5	3.58(17)	923.1	3750.6	0.79(10)	1401.7	2351.6	2.54(15)	(2415.3)		<0.3
505.5	1989.0	13.45(29)	931.0	2414.5	6.23(20)	1417.4	1483.5	5.48(21)	(2608.4)		<0.3
523.5	3750.6	2.82(15)	949.8	949.7	5.64(18)	1464.8	2414.5	0.32(9)	(2747.3)		<0.3
527.3 <sup>d</sup>	2253.3	0.63(33)	992.2	992.2	26.24(55)	1483.6	1483.5	14.33(41)	(2874.9)		<0.3
527.3 <sup>d</sup>	2516.3	0.87(30)	(1010.8)		0.98(13)	1522.0	3775.3	1.16(13)	(3032.1)		0.43(11)
533.7	1483.5	6.96(21)	1037.8	3750.6	0.60(14)	1600.5	2592.5	1.47(13)	(3063.4)		<0.3
573.2	2924.8	3.10(18)	1101.5	2827.5	1.00(12)	(1623.9)		0.75(11)	(3167.2)		<0.3
590.9	3005.4	2.14(15)	1130.4	3963.9	0.58(10)	1664.0	3651.5	0.47(12)	(3677.7)		0.32(8)
603.1	2592.5	2.14(18)	1158.6	3963.9	1.43(13)	1680.4	1680.4	4.22(21)	(3697.1)		0.30(8)
614.5	3750.6	2.23(15)	1190.5	2674.0	0.58(11)	(1772.3)		0.34(10)	(3986.7)		0.51(9)
734.1 <sup>d</sup>	1726.1	1.22(49)	1229.4	2712.9	3.57(16)	1811.3	2805.4	1.06(13)			

<sup>a</sup> Uncertainties are within 1 keV

<sup>b</sup> Assuming pure  $E2$  multipolarity

<sup>c</sup> Assuming pure  $M1$  multipolarity

<sup>d</sup> Doublet

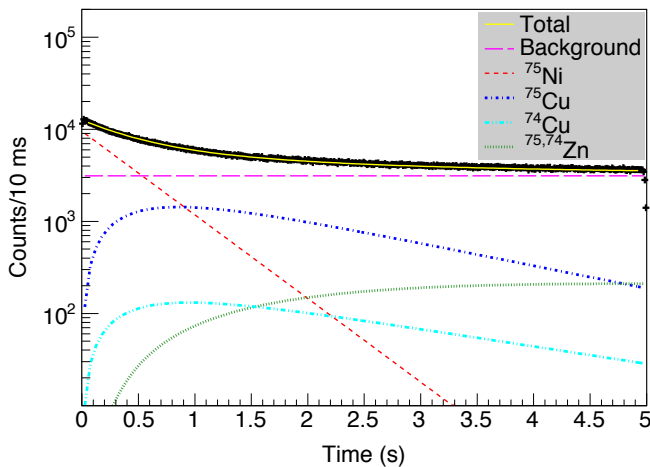


FIG. 2. (Color online) Time difference between implantation of  $^{75}\text{Ni}$  ions and detection of electrons inside the area of spatial correlation. The various curves show the fit of contributions from individual decays based on known half-lives and probability for beta-delayed neutron emission (see text for more details).

sidered. Evaluated half-lives for  $^{75,74}\text{Cu}$  and  $^{75,74}\text{Zn}$  [32] and the reported  $\beta$ -delayed neutron emission probability for  $^{75}\text{Ni}$  [31] were used as fixed parameters in the fit.

The half-life of  $^{75}\text{Ni}$ ,  $T_{1/2} = 331.6(32)$  ms, was obtained from the present experimental data by gating on the 992, 884 and 1484 keV transitions [27, 29]. A total number of  $4.53(3) \times 10^5$   $^{75}\text{Ni}$   $\beta$ -decays in a time window of 2.5 s after implantation of the ions was obtained after removing all contributions from background and subsequent decays. The method for fitting the decay curve is explained in more detail in Ref. [27].

The quality and amount of data allowed performing a  $\gamma$ - $\gamma$  coincidence analysis. Figure 3 shows background-subtracted  $\gamma$ -ray spectra gated on the four strongest transitions of 992, 884, 1484 and 506 keV. The level scheme shown in Fig. 5 was constructed based on coincidence relations between the transitions, their energy sums and differences, and their intensities. From the intensities of the transitions,  $\log ft$  values were obtained using  $T_{1/2} = 331.6(32)$  ms [27, 29] and  $Q_{\beta^-} = 10230(300)$  keV [34]. A total of 71.6(35)% of the  $\beta$ -decay events were found to feed the excited states of  $^{75}\text{Cu}$  that are included in the level scheme of Fig. 5, while 11.6(3)% of the events were found to feed excited states of  $^{74}\text{Cu}$  through the emission of  $\beta$ -delayed neutrons. The latter value can only be considered a lower limit for the  $\beta$ -delayed neutron emission probability, because the  $\beta$ -delayed neutron branch feeding the ground state of  $^{74}\text{Cu}$  is unknown. Based on these values, a maximum of 20.6% of  $\beta$ -decay intensity could directly feed the ground states in  $^{75}\text{Cu}$  or  $^{74}\text{Cu}$ .

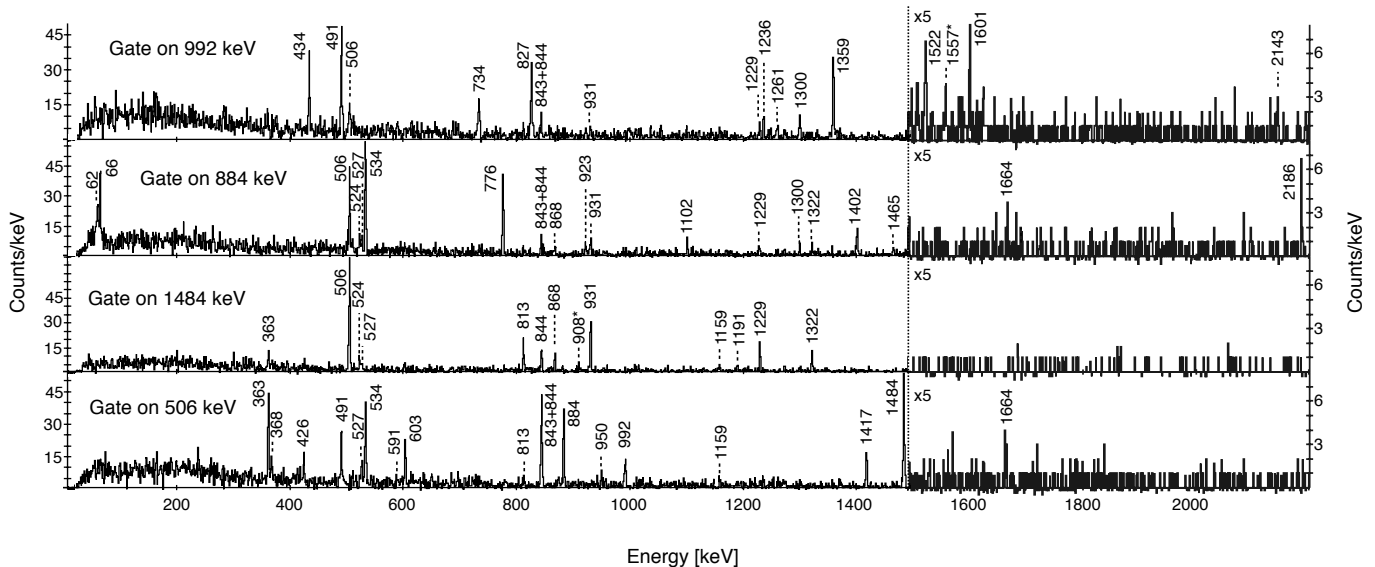


FIG. 3. Background-subtracted  $\gamma$ -ray spectra gated on the four strongest transitions of  $^{75}\text{Cu}$  with energies 992, 884, 1484, and 506 keV. All transitions which are labeled by their energy have been placed in the level scheme of Fig. 5, except those at 908 and 1557 keV (labeled by  $\star$ ).

230 A further 9.3(10)% of the absolute  $\gamma$ -ray intensity was  
 231 tentatively assigned to  $^{75}\text{Cu}$ , but could not be placed  
 232 in the level scheme (see Table I). If it is assumed that  
 233 all these unplaced transitions directly feed the ground  
 234 state of  $^{75}\text{Cu}$ , the unobserved  $\beta$ -decay feeding decreases  
 235 to 8(4)%.

236 The spin assignments in Fig. 5 are based on the known  
 237  $5/2^-$  ground-state spin-parity of  $^{75}\text{Cu}$  [5, 6] and the pos-  
 238 sible multiplicities of the  $\gamma$ -ray transitions, the system-  
 239 atics of the odd-A Cu isotopes between  $^{69}\text{Cu}$  and  $^{79}\text{Cu}$ ,  
 240 and the comparison with theoretical calculations, which  
 241 will be discussed in Section IV. The only exception is  
 242 the  $7/2^-$  state at 1680 keV, for which the spin and par-  
 243 ity assignment was mostly based on the results of the  
 244 shell model calculations (see Sec. IV C). All the excited  
 245 states with assigned spin values were assigned a nega-  
 246 tive parity. Although the measured  $\log ft$  values can  
 247 not be used as a firm criterion to perform spin and par-  
 248 ity assignments (because of the large systematic error in  
 249 the  $\beta$ -decay branching ratios related to the unplaced  $\beta$ -  
 250 decay intensity), those states with  $\log ft$  values which are  
 251 only consistent with allowed decays ( $\log ft < 6$ ), appear  
 252 above 2.5 MeV, suggesting the occurrence of positive-  
 253 parity states at these energies, in agreement with the  
 254 systematics [8, 35].

255 The time window for the  $\beta$ - $\gamma$  coincidences was suf-  
 256 ficiently long to observe the previously known isomeric  
 257 61.8 and 66.2 keV transitions with half-lives of 310(8)  
 258 and 149(6) ns, respectively [18, 19], in coincidence with  
 259 other transitions. Figure 4 shows the low-energy part  
 260 of the background-subtracted  $\gamma$ -ray spectra gated on the  
 261 884, 950, 1417, and 1484 keV transitions. The presence  
 262 of lines at 61.8 and 66.2 keV in the spectra gated on the  
 263 884 and 1417 keV transitions, together with their non-

264 observation in the spectra gated on the 950 and 1484  
 265 keV transitions, respectively, fixes the positions of the  
 266 61.8 and 66.2 keV states, in agreement with the more  
 267 recent works in Refs. [19, 20] and in disagreement with  
 268 the earlier work in Ref. [18]. It should be noticed that  
 269 the energy difference between the 950 and the 884 keV  
 270 transitions and between the 1484 and the 1417 keV tran-  
 271 sitions matches the energy of the 66.2 keV transition.

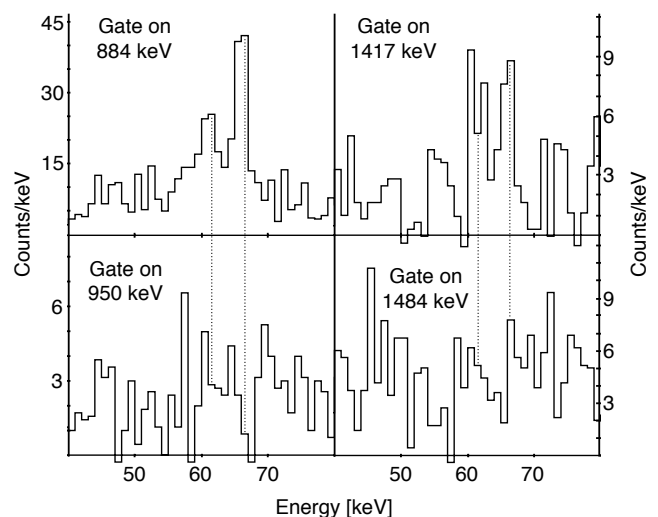


FIG. 4. Background-subtracted  $\gamma$ -ray spectra gated on the 884, 950, 1417, and 1484 keV transitions in the energy range of the two isomeric transitions of 61.8 and 66.2 keV.

The fact that the 884 and the 1417 keV transitions are

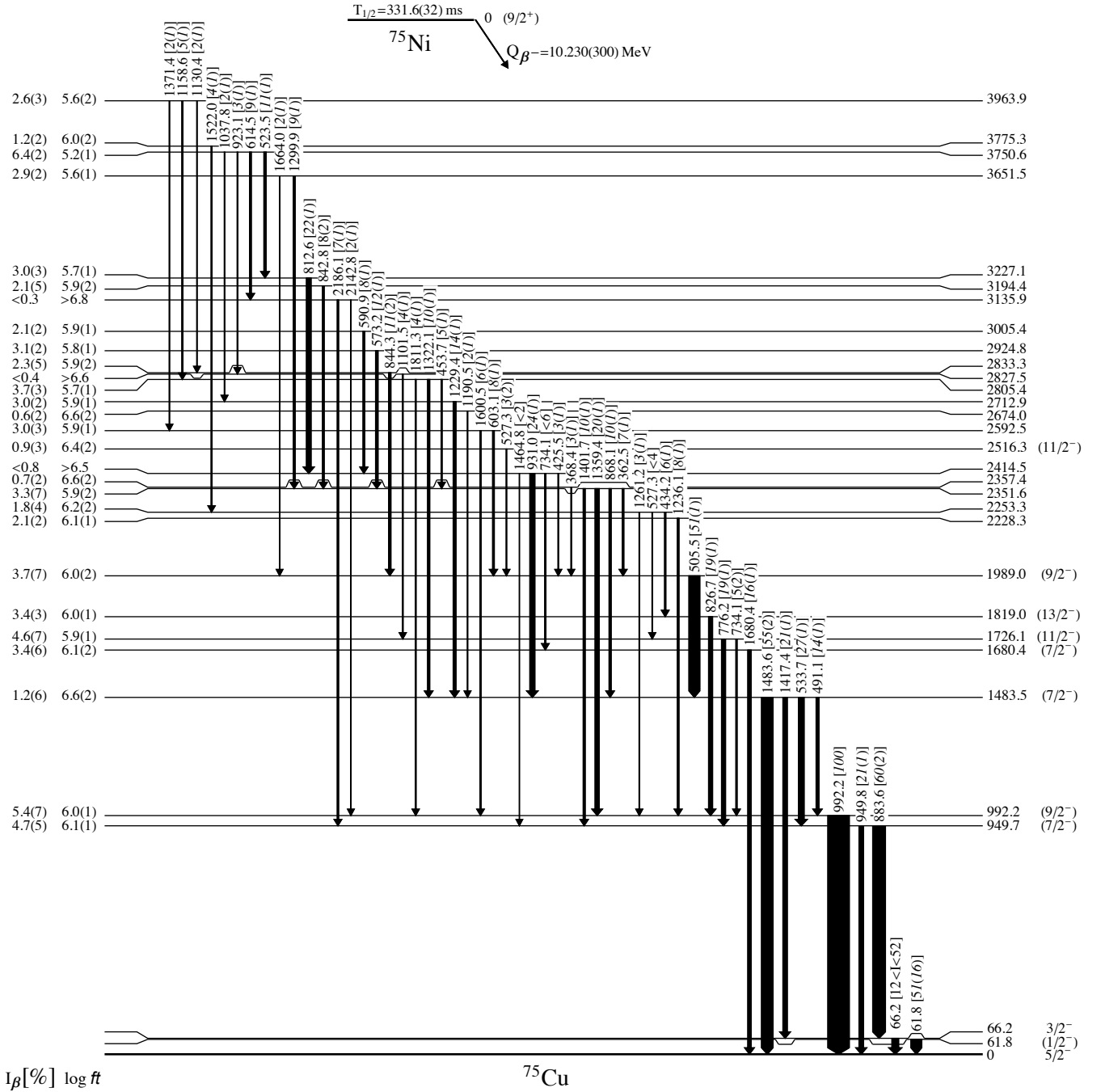


FIG. 5. Level scheme of  $^{75}\text{Cu}$ . The energies of the states and the transitions are given in keV, and the uncertainties are within 1 keV. The relative intensities of the transitions (in brackets) are normalized to the 992 keV transition and corrected for internal conversion. Lower and upper limits are given for the relative intensity of the 66.2 keV transition. For the discussion of the  $\beta$ -decay branching ratios ( $I_{\beta}$ ) to the 61.8 and 66.2 keV states, and to the ground state, see the text (Section III).

273 in coincidence with the 61.8 keV transition, implies the  
 274 existence of an intense low-energy transition of 4.4(6) keV  
 275 connecting the two isomers, which was already discussed  
 276 by Petrone *et al.* [19]. Without any isomeric states re-  
 277 ported for the parent nucleus  $^{75}\text{Ni}$ , all  $\beta$ -decays are as-  
 278 sumed to originate from its ground state, which has a pro-  
 279 posed  $9/2^+$  spin and parity. Therefore, based on the pro-  
 280 posed spin and parities of the isomers, (see Section IV),  
 281 there should be no direct  $\beta$ -decay feeding of these states.  
 282 Since no direct  $\gamma$ -ray feeding of the state at 61.8 keV ex-  
 283 citation energy was observed, all feeding into this 61.8  
 284 keV state should therefore proceed through the 4.4 keV  
 285 transition. The absence of direct  $\beta$ -decay feeding of these  
 286 states could not be experimentally confirmed due to the

287 large uncertainties for the intensities of the 61.8 and 66.2  
 288 keV transitions and the non-observation of the 4.4 keV  
 289 transition.

#### 290 IV. DISCUSSION

291 In the low-lying level structure of odd-mass Cu iso-  
 292 topes, which in a normal occupation scheme have only  
 293 one proton outside the  $Z = 28$  shell gap, the occupa-  
 294 tion of the  $1f_{5/2}$ ,  $2p_{3/2}$ , or  $2p_{1/2}$  orbitals by the unpaired  
 295 proton will give rise to  $5/2^-$ ,  $3/2^-$ , and  $1/2^-$  states  
 296 with single-particle nature. The same proton above the  
 297  $Z = 28$  shell gap could also couple to excited states in  
 298 the corresponding even-even Ni cores, creating particle-  
 299 core coupled multiplets. Furthermore, the presence of  
 300  $7/2^-$  states with proton-hole  $1f_{7/2}^{-1}$  configurations at rela-  
 301 tively low energies, could be favored in isotopes with  
 302  $N \geq 40$  because of the reduction of the  $Z = 28$  shell gap  
 303 with the filling of the  $\nu 1g_{9/2}$  orbital, and the occurrence  
 304 of quadrupole correlations between excited protons and  
 305  $\nu 1g_{9/2}$  neutrons [2, 4, 7, 36–38]. In the following sections,  
 306 the low-lying level structure of  $^{75}\text{Cu}$  is discussed in the  
 307 context of the systematics of the  $N \geq 40$  odd-mass Cu  
 308 isotopes.

309 To help identifying the populated low-lying states,  
 310 and to better understand the level structure of  $^{75}\text{Cu}$ ,  
 311 Monte Carlo shell model (MCSM) calculations were per-  
 312 formed in the present work. The MCSM calculations  
 313 used the A3DA interaction [37, 39], which is built on the  
 314  $pf_{g9/2}d_{5/2}$  model space for both neutrons and protons,  
 315 assuming  $^{40}\text{Ca}$  as inert core. Those experimental energy  
 316 states with assigned spin and parity are shown in Fig. 6  
 317 together with the corresponding calculated energy states.  
 318 The agreement with the experimental levels is good. For  
 319 each of these states, occupation numbers are shown in Ta-  
 320 ble II. The composition of their wave function was eval-  
 321 uated in terms of the probability of coupling one proton  
 322 in the  $1f_{7/2}$ ,  $1f_{5/2}$ ,  $2p_{3/2}$ , or  $2p_{1/2}$  orbitals to different  
 323 energy states in the  $^{74}\text{Ni}$  core.  $B(E2, M1)$  values, elec-  
 324 tric quadrupole, and magnetic moments were calculated.  
 325 Furthermore, the shapes of the MCSM basis vectors for  
 326 each state were calculated, and are shown in Fig. 7 to-  
 327 gether with the potential energy surface (PES) of the nu-  
 328 cleus. Some of the results from the MCSM calculations  
 329 have been previously reported for  $^{75}\text{Cu}$  [20],  $^{77}\text{Cu}$  [7] and  
 330  $^{79}\text{Cu}$  [17]. Occupation numbers corresponding to excited  
 331 states in  $^{77}\text{Cu}$  are shown in Table III.

##### 332 A. The $5/2^-$ , $3/2^-$ and $1/2^-$ states.

333 The first  $5/2^-$  and  $3/2^-$  states in odd-mass Cu iso-  
 334 topes with  $N \geq 40$  have been associated with  $\pi 1f_{5/2}$   
 335 and  $\pi 2p_{3/2}$  single-particle configurations, respectively [7,  
 336 8, 17]. The predominant single-particle character of these  
 337 states in  $^{69-73}\text{Cu}$  was indicated by measuring relatively

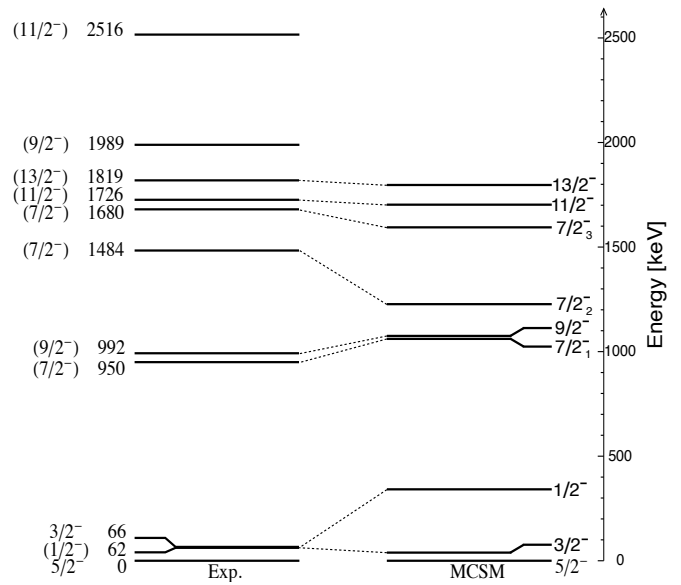


FIG. 6. (left): Experimental energy states of  $^{75}\text{Cu}$  with assigned spins and parities. (right): MCSM calculations.

338 low  $B(E2; 5/2^- \rightarrow 3/2^-_{gs})$  values ( $< 5$  W.u.) [9]. Spec-  
 339 troscopic factors measured in  $(d, ^3\text{He})$  and  $(\bar{t}, \alpha)$  reac-  
 340 tions [40–43] established the spin and parity of the  $5/2^-$   
 341 states in  $^{69,71}\text{Cu}$ , and confirmed the  $\pi 1f_{5/2}$  and  $\pi 2p_{3/2}$   
 342 single-particle character of the  $5/2^-$  states and the  $3/2^-$   
 343 ground states, respectively. The significant deviations  
 344 from the effective Schmidt estimates of the magnetic mo-

TABLE II. Occupation numbers of proton and neutron orbits of calculated excited states of  $^{75}\text{Cu}$ .

$J_n^\pi$	$\pi f_{7/2}$	$\pi p_{3/2}$	$\pi f_{5/2}$	$\pi p_{1/2}$	$\pi g_{9/2}$	$\pi d_{5/2}$
$1/2^-$	7.62	0.45	0.66	0.20	0.05	0.01
$3/2^-$	7.65	0.86	0.35	0.08	0.06	0.01
$5/2^-$	7.62	0.34	0.90	0.07	0.05	0.01
$7/2^-_1$	7.64	0.77	0.43	0.10	0.06	0.01
$7/2^-_2$	6.71	0.62	1.37	0.22	0.07	0.01
$7/2^-_3$	7.55	0.50	0.83	0.05	0.05	0.01
$9/2^-$	7.64	0.34	0.87	0.09	0.05	0.01
$11/2^-$	7.66	0.83	0.36	0.08	0.06	0.01
$13/2^-$	7.66	0.30	0.91	0.08	0.05	0.01
	$\nu f_{7/2}$	$\nu p_{3/2}$	$\nu f_{5/2}$	$\nu p_{1/2}$	$\nu g_{9/2}$	$\nu d_{5/2}$
$1/2^-$	7.97	3.90	5.88	1.90	6.06	0.31
$3/2^-$	7.97	3.88	5.85	1.89	6.21	0.21
$5/2^-$	7.97	3.87	5.83	1.84	6.28	0.23
$7/2^-_1$	7.97	3.92	5.91	1.93	6.01	0.26
$7/2^-_2$	7.97	3.87	5.75	1.86	6.21	0.34
$7/2^-_3$	7.97	3.90	5.86	1.89	6.18	0.19
$9/2^-$	7.97	3.92	5.91	1.93	6.00	0.26
$11/2^-$	7.97	3.93	5.94	1.95	5.96	0.24
$13/2^-$	7.97	3.93	5.93	1.94	5.98	0.24

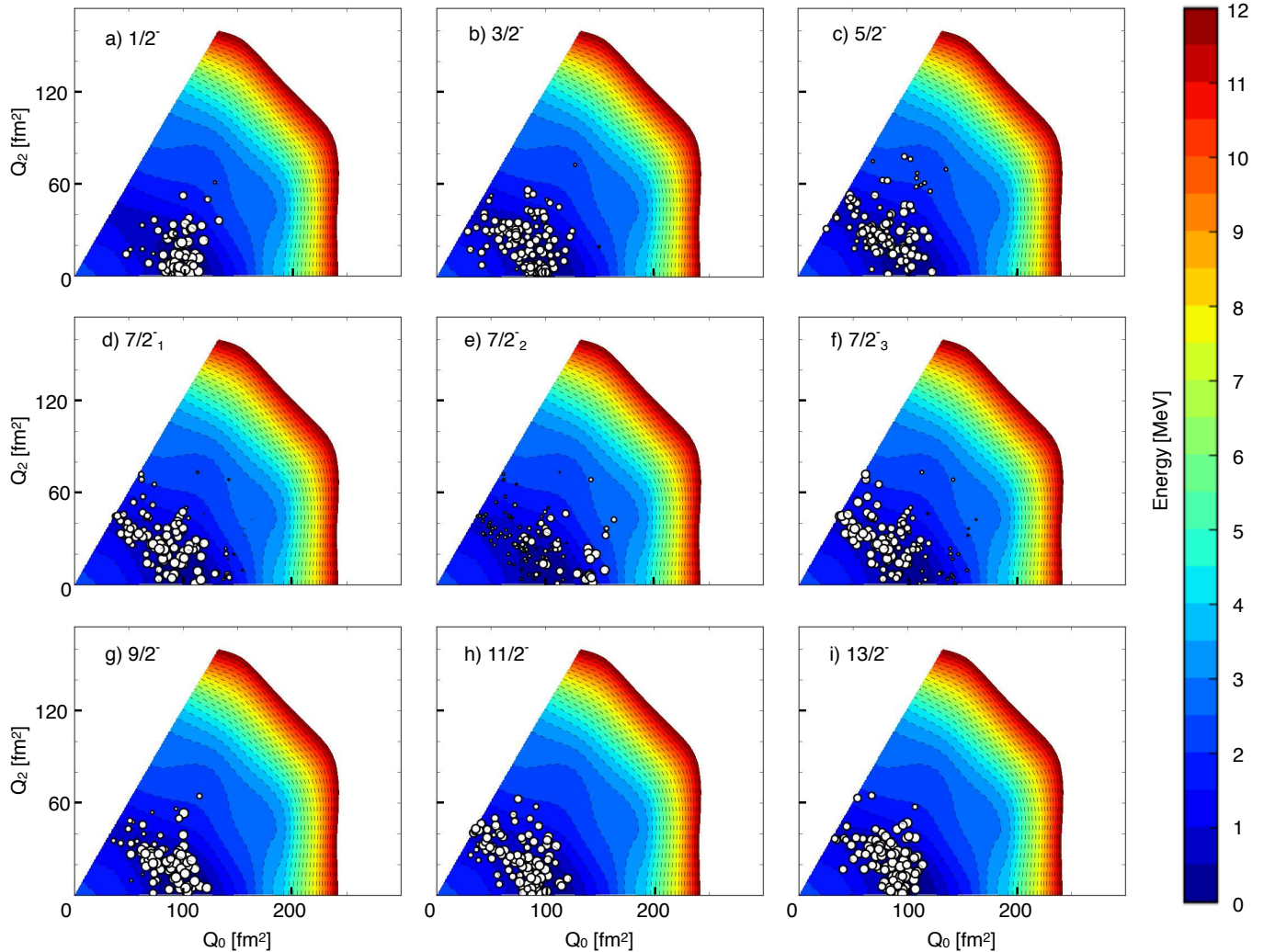


FIG. 7. (Color online) The circles drawn on the potential energy surface of the nucleus indicate the shapes of the MCSM basis vectors of calculated excited states of  $^{75}\text{Cu}$ . See Ref. [37] for details.

ments measured for the ground states in  $^{73,75}\text{Cu}$  [5, 6] and the excited  $3/2^-$  state in  $^{75}\text{Cu}$  [20] are interpreted as a consequence of the enhanced collectivity in the  $^{72,74}\text{Ni}$  cores [20].

The systematics of the energies of the first  $5/2^-$  and  $3/2^-$  states in  $^{69-77}\text{Cu}$  can be seen in Fig. 9. The ground-state spin changes from  $3/2^-$  in the lighter isotopes ( $A \leq 73$ ) to  $5/2^-$  in the heavier ones [5, 6]. The excited  $3/2^-$  state is also known in  $^{79}\text{Cu}$  [17]. In  $^{75}\text{Cu}$ , where the inversion of these energy states occurs, the isomeric  $3/2^-$  state lies very close to the ground state [18–20]. The other isomer, at just 4.4 keV below the  $3/2^-$  state, has been assigned  $1/2^-$  spin and parity, based on systematics of the  $1/2^-$  states in the lighter isotopes [18, 19] (see Fig. 8), and the results of the time-differential perturbed angular distribution measurements [20]. In the present  $\beta$ -decay experiment, no direct  $\gamma$ -ray feeding of the state at 61.8 keV was observed, while the state at 66.2 keV

was directly fed by two transitions with 884 and 1417 keV. This feeding pattern is consistent with spin-parity  $3/2^-$  for the state at 66.2 keV, which is fed by  $E2$  transitions from  $7/2^-$  states above, whereas spin-parity  $1/2^-$  for the state at 61.8 keV explains the non-observation of any feeding from higher-spin states due to the high multipolarity that would be required.

The MCSM calculations find the  $5/2^-$  ground state and the first  $3/2^-$  state of  $^{75}\text{Cu}$  to have a predominant single-particle character, which has been now experimentally verified in Ref. [21] for both  $^{75}\text{Cu}$  and  $^{77}\text{Cu}$ . The  $5/2^-$  state is found to have an occupation number of 0.90 in the  $\pi 1f_{5/2}$  orbital, and its wave function becomes purer towards the end of the neutron  $fp$  shell, with the occupation number increasing to 0.99 in  $^{77}\text{Cu}$  and 1.05 in  $^{79}\text{Cu}$ . The energy of the  $3/2^-$  state in  $^{75}\text{Cu}$  is well reproduced by the model (see Fig. 6), and the  $B(E2; 3/2^- \rightarrow 5/2^-)$  value was calculated to

TABLE III. Occupation numbers of proton and neutron orbits of calculated excited states of  $^{77}\text{Cu}$ .

$J_n^\pi$	$\pi f_{7/2}$	$\pi p_{3/2}$	$\pi f_{5/2}$	$\pi p_{1/2}$	$\pi g_{9/2}$	$\pi d_{5/2}$
$1/2^-$	7.61	0.30	0.84	0.20	0.04	0.01
$3/2^-$	7.67	0.88	0.35	0.05	0.05	0.01
$5/2^-$	7.64	0.27	0.99	0.05	0.04	0.01
$7/2_1^-$	7.65	0.76	0.48	0.05	0.05	0.01
$7/2_2^-$	6.68	0.55	1.54	0.16	0.07	0.01
$7/2_3^-$	7.64	0.64	0.65	0.03	0.04	0.01
$9/2_1^-$	7.66	0.25	0.99	0.05	0.04	0.01
$9/2_2^-$	6.72	0.56	1.47	0.19	0.06	0.01
$11/2^-$	7.70	0.66	0.55	0.03	0.05	0.01
$13/2^-$	7.71	0.27	0.95	0.03	0.04	0.01
$\nu f_{7/2}$	$\nu p_{3/2}$	$\nu f_{5/2}$	$\nu p_{1/2}$	$\nu g_{9/2}$	$\nu d_{5/2}$	
$1/2^-$	7.98	3.95	5.96	1.95	7.84	0.31
$3/2^-$	7.98	3.93	5.93	1.93	8.02	0.21
$5/2^-$	7.98	3.92	5.92	1.89	8.05	0.23
$7/2_1^-$	7.99	3.96	5.97	1.97	7.87	0.24
$7/2_2^-$	7.99	3.94	5.94	1.95	7.87	0.31
$7/2_3^-$	7.99	3.96	5.96	1.96	7.91	0.22
$9/2_1^-$	7.99	3.97	5.97	1.97	7.86	0.24
$9/2_2^-$	7.99	3.96	5.96	1.96	7.80	0.33
$11/2^-$	7.99	3.98	5.99	1.98	7.88	0.19
$13/2^-$	7.99	3.98	5.99	1.98	7.88	0.18

381 be 4.2 W.u., in good agreement with the systematics [9].  
 382 For the  $3/2^-$  state, the occupation number of the  $\pi 2p_{3/2}$   
 383 orbital is calculated to be 0.86, increasing to 0.88 in  $^{77}\text{Cu}$   
 384 and 1.02 in  $^{79}\text{Cu}$ , in disagreement with the previous cal-  
 385 culations of Ref. [4]. The PES of  $^{75}\text{Cu}$  shown in Fig. 7  
 386 shows a considerable degree of  $\gamma$ -softness with a very  
 387 wide minimum on the prolate side around  $Q_0 = 100 \text{ fm}^2$   
 388 ( $\beta \sim 0.2$ ), and it is similar to the PES of  $^{74}\text{Ni}$ , shown in  
 389 Ref. [37].

390 The systematics of the energies of the first  $1/2^-$  states,  
 391 and the  $B(E2; 1/2^- \rightarrow g.s.)$  values in  $^{69-79}\text{Cu}$  are shown  
 392 in Fig. 8. The  $1/2^-$  spin and parity have only been  
 393 measured in  $^{69}\text{Cu}$ , using transfer reactions [40–42]. The  
 394 relatively large  $B(E2)$  values observed in  $^{71-75}\text{Cu}$  indi-  
 395 cate a collective nature of the  $1/2^-$  states in these iso-  
 396 topes [9, 19]. In the case of  $^{77}\text{Cu}$ , the  $1/2^-$  state was not  
 397 identified in the  $\beta$ -decay of  $^{77}\text{Ni}$  [7], which suggests that it  
 398 lies above the  $3/2^-$  state at 293 keV. In  $^{75}\text{Cu}$ , the MCSM  
 399 finds that the wave function of the  $1/2^-$  state is domi-  
 400 nated by the  $|\pi 1f_{5/2} \otimes 2_1^+\rangle$  configuration (40%). The  
 401 calculated  $B(E2)$  value agrees very well with the experi-  
 402 mental result, and the collectivity is expected to decrease  
 403 towards the shell closure, with the occupation number of  
 404 the  $\pi 2p_{1/2}$  orbital rapidly increasing from 0.20 in  $^{75}\text{Cu}$   
 405 and  $^{77}\text{Cu}$  to 0.62 in  $^{79}\text{Cu}$ . The maximum of collectivity  
 406 in  $^{73,75}\text{Cu}$  can be interpreted in connection to the fact  
 407 that the  $\nu 1g_{9/2}$  orbital is approximately half-filled, en-  
 408 hancing the occurrence of  $\pi 1f_{5/2} - \nu 1g_{9/2}$  quadrupole  
 409 correlations. As has been discussed in Refs. [7, 20],  
 410 these correlations account as well for the lowering of the  
 411  $5/2^-$  state below the  $3/2^-$  state in  $^{75}\text{Cu}$ , explaining the  
 412 change of the ground-state before the calculated cross-

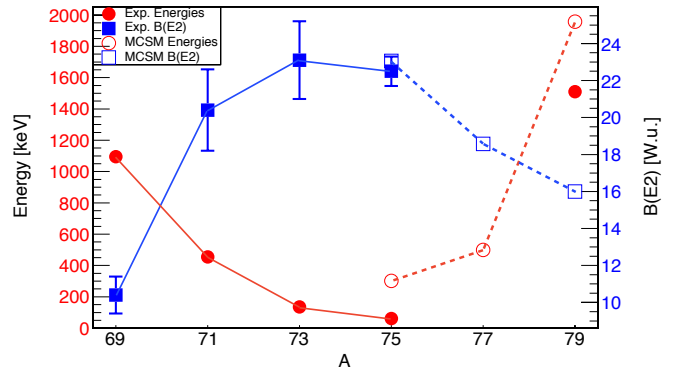


FIG. 8. (Color online) Systematics of the energies of the first  $1/2^-$  states (red circles), and  $B(E2; 1/2^- \rightarrow g.s.)$  values (blue squares) in odd-A  $^{69-79}\text{Cu}$  isotopes [9, 17, 19]. Results from the MCSM calculations (open symbols) are shown together with experimental values (filled symbols). For  $^{79}\text{Cu}$ , the assignment of the  $1/2^-$  state was based on the results of the MCSM calculations (see Ref. [17]).

413 ing of the  $\pi 1f_{5/2}$  and  $\pi 2p_{3/2}$  ESPEs in  $^{77}\text{Cu}$ . The  $1/2^-$   
 414 state is found by the calculations to have an average  
 415 prolate shape (Fig. 7(a)), in contrast to the  $3/2^-$  and  
 416 the  $5/2^-$  states, for which the circles in Figs. 7(b) and  
 417 (c), respectively, are distributed along the  $\gamma$ -coordinate.  
 418 For the  $1/2^-$  state, there is also a slight enhancement  
 419 in occupation of the  $\nu d_{5/2}$  orbital, which suggests that  
 420  $\pi 2f_{1/2} - \nu 2d_{5/2}$  quadrupole correlations play a roll in the  
 421 collectivity of this state.

## B. Particle-core coupling states.

422  
 423 The systematics of the energies and decay sequences  
 424 of particle-core coupling states observed in odd-mass  
 425  $^{69-77}\text{Cu}$  isotopes are shown in Fig. 9 and Fig. 10, includ-  
 426 ing the results from the  $\beta$ -decay study of  $^{77}\text{Cu}$  [7] and the  
 427 results obtained in this work. The  $7/2^-$  state at 1871 keV  
 428 in  $^{69}\text{Cu}$ , is known from transfer [40–42] and multi-nucleon  
 429 transfer [13] reactions, while the assigned  $7/2^-$  states at  
 430 1189 and 961 keV in  $^{71,73}\text{Cu}$ , respectively, were identi-  
 431 fied in the  $\beta$ -decay study of Ref. [8]. As can be observed  
 432 in Fig. 9, the energies of these states follow closely the  
 433 energies of the first  $2_1^+$  states of  $^{68-72}\text{Ni}$ . In Ref. [9],  
 434 Stefanescu *et al.* showed that the  $B(E2; 7/2^- \rightarrow 3/2^-)$   
 435 values of these states in  $^{69,71}\text{Cu}$  are also very similar to  
 436 the  $B(E2; 2_1^+ \rightarrow 0_1^+)$  values measured in the correspond-  
 437 ing  $^{68,70}\text{Ni}$  cores;  $^{73}\text{Cu}$  is the exception, as the mea-  
 438 sured  $B(E2; 7/2^- \rightarrow 3/2^-) = 14.9(18)$  W.u. [9] is  $\sim 3.5$   
 439 times larger than the  $B(E2; 2_1^+ \rightarrow 0_1^+)$  value measured  
 440 in  $^{72}\text{Ni}$  [53]. These  $7/2^-$  states have been associated  
 441 with the  $|\pi 2p_{3/2} \otimes 2_1^+\rangle$  configuration [54]. For  $^{69,71}\text{Cu}$ ,  
 442  $\Delta I = 2$  bands have been observed on top of the  $7/2^-$   
 443 states [11, 13, 14]. The  $11/2^-$  members of these bands  
 444 can be associated with the  $|\pi 2p_{3/2} \otimes 4_1^+\rangle$  configuration.

Two states in  $^{75}\text{Cu}$  were found lying very close to the  $2_1^+$  state of  $^{74}\text{Ni}$ . The state at 950 keV decays to both the  $3/2^-$  and the  $5/2^-$  ground state, and the 884 keV transition to the  $3/2^-$  state is 3 times stronger. The state at 992 keV, on the other hand, does not decay to the  $3/2^-$  state, but only to the ground state. Based on the systematics shown in Fig. 10, the state at 950 keV is assigned  $7/2^-$  spin and parity, and can be associated with the  $|\pi 2p_{3/2} \otimes 2_1^+\rangle$  configuration. The state at 992 keV, which can be associated with the  $|\pi 1f_{5/2} \otimes 2_1^+\rangle$  configuration, is thus assigned  $9/2^-$  spin and parity. States at 1726 and 1819 keV were also found very close to the  $4_1^+$  state of  $^{74}\text{Ni}$ ; the state at 1726 keV decays to the  $7/2^-$  state with a transition about 4 times stronger than the transition to the  $9/2^-$  state, while the 1819 keV state only decays to the  $9/2^-$  state. These two states at 1726 and 1819 keV are thus assigned  $11/2^-$  and  $13/2^-$  spin and parity, respectively, and could correspond to the  $|\pi 2p_{3/2} \otimes 4_1^+\rangle$  and  $|\pi 1f_{5/2} \otimes 4_1^+\rangle$  configurations, respectively. The energies of the  $7/2^-$ ,  $9/2^-$ ,  $11/2^-$  and  $13/2^-$  particle-core coupling states are well reproduced by the MCSM (see Fig. 6). The  $3/2^-$ ,  $7/2_1^-$  and  $11/2^-$  states, as well as the  $5/2^-$ ,  $9/2^-$  and  $13/2^-$  states, are found to have very

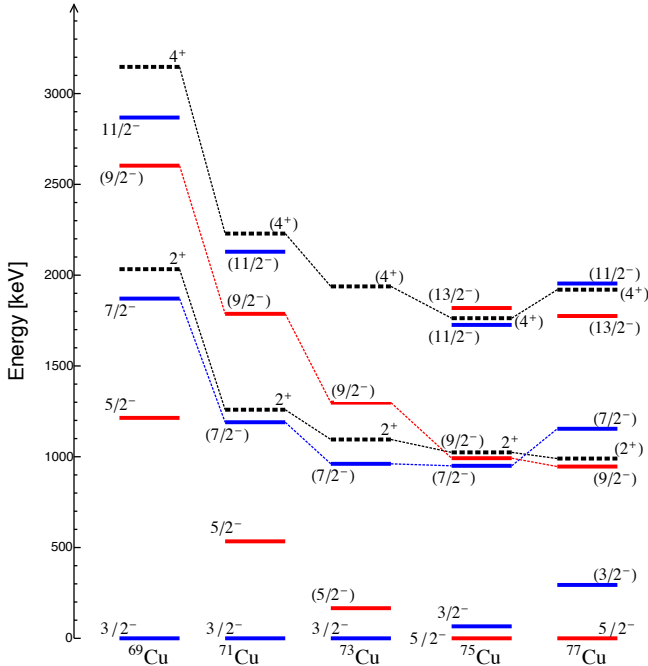


FIG. 9. (Color online) Systematics of the energies of particle-core coupling states in odd-A  $^{69-77}\text{Cu}$  isotopes [7, 8, 14]. The levels corresponding to the Ni cores [44–51] are shown in dashed lines. The  $3/2^-$ ,  $7/2^-$  and  $11/2^-$  states (in blue), can be associated with the  $|\pi 2p_{3/2} \otimes 0_1^+, 2_1^+, 4_1^+\rangle$  configurations, respectively, while the  $5/2^-$ ,  $9/2^-$  and  $13/2^-$  states (in red) can be associated with the  $|\pi 1f_{5/2} \otimes 0_1^+, 2_1^+, 4_1^+\rangle$  configurations, respectively. In  $^{73}\text{Cu}$ , the spin assignment of the state at 1287 keV is not clear, but the systematics suggest an important  $|\pi 1f_{5/2} \otimes 2_1^+\rangle$  component in its wave function.

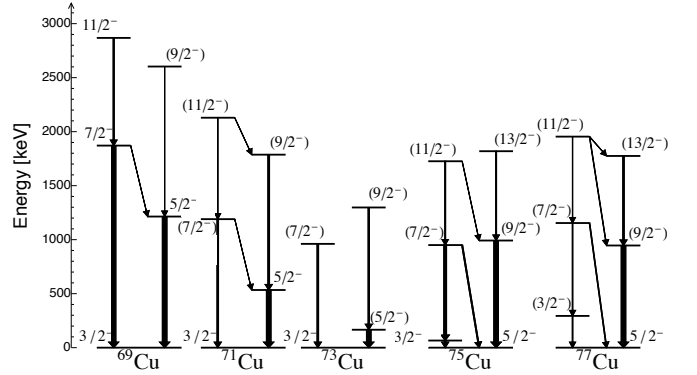


FIG. 10. Systematics of the decay sequences of particle-core coupling states in odd-A  $^{69-77}\text{Cu}$  isotopes [7, 8, 14]. The widths of the transitions correspond with the relative intensities, normalized to the strongest transition shown in each isotope. In  $^{71}\text{Cu}$ , the  $11/2^- \rightarrow 9/2^-$  transition has only been observed in Ref. [14] and its intensity was normalized according to the observed branching ratio.

similar occupation numbers (see Table II), respectively, supporting their particle-core coupling character. Their average deformation (see Fig. 7) is found to be very similar to that of the  $0_1^+$  and  $2_1^+$  states of  $^{74}\text{Ni}$  (Ref. [37]). Furthermore, the MCSM calculates  $B(E2; 9/2^- \rightarrow 5/2^-) = 9.6$  W.u. and  $B(E2; 7/2^- \rightarrow 3/2^-) = 8.0$  W.u., values that are very similar to the measured  $B(E2; 2_1^+ \rightarrow 0_1^+) = 7.1(23)$  W.u. in  $^{74}\text{Ni}$  [50]. An excited state was observed in the experiment at 1680 keV, which only decays directly to the ground state. This state can be associated with the  $7/2_3^-$  state found by the MCSM calculations at a very similar energy (see Fig. 6), which is composed by the mixing of several configurations:  $|\pi 1f_{5/2} \otimes 2_1^+\rangle$  (32%),  $|\pi 1f_{5/2} \otimes 2_2^+\rangle$  (27%),  $|\pi 2p_{3/2} \otimes 4_2^+\rangle$  (11%), etc.

The  $9/2^-$   $|\pi 1f_{5/2} \otimes 2_1^+\rangle$  states in  $^{69-73}\text{Cu}$  have not yet been firmly established. In  $^{71}\text{Cu}$ , a state at 1786 keV was first observed in fragmentation [11] and multi-nucleon transfer reactions [12], and a  $9/2^+$  spin and parity was proposed in the latter work; afterwards, Franchoo *et al.* [8] proposed a  $|\pi 1f_{5/2} \otimes 2_1^+\rangle$  configuration for this state, together with another possible member of the same multiplet observed at 1846 keV, but the proposed  $9/2^-$  and  $7/2^-$  spins and parities for these two states were not unambiguously assigned. Later, in another multi-nucleon transfer experiment [14], the state at 1786 keV was found to be connected with the  $11/2^-$   $|\pi 2p_{3/2} \otimes 4_1^+\rangle$  state (as shown in Fig. 10) and assigned a  $9/2^-$  spin and parity. For  $^{69}\text{Cu}$ , in the  $\beta$ -decay experiment of Ref. [8], a  $9/2^-$  state was proposed at 2603 keV, but it was suggested to have a different configuration based on the comparison with the shell-model calculations presented in Ref. [13]. In  $^{73}\text{Cu}$ , Franchoo *et al.* [8] proposed the observed state at 1297 keV to have a  $|\pi 1f_{5/2} \otimes 2_1^+\rangle$  configuration, with possible  $9/2^-$  or  $7/2^-$  spins and parity; however, a very low  $B(E2)$  value measured later for its decay to the  $5/2^-$  state ( $< 2$  W.u.), and the comparison with shell

504 model calculations suggested a  $5/2^-$  spin and parity as-  
 505 signment for this state, and a mixed  $|\pi 1f_{5/2} \otimes 0_1^+, 2_1^+\rangle$   
 506 configuration [10]. These states have been included in  
 507 Figs. 9 and 10, and the observed trend in their energies,  
 508 very similar to the trend followed by the  $5/2^-$  sates, to-  
 509 gether with their decay patterns, suggest an important  
 510  $|\pi 1f_{5/2} \otimes 2_1^+\rangle$  component in their wave functions. In the  
 511 case of  $^{73}\text{Cu}$ , the relatively long lifetime measured for  
 512 this state in Ref. [10] could be related to unaccounted  
 513 side feeding from long-lived states.

### 514 C. The intruder band.

515 In  $^{69-73}\text{Cu}$ , other  $7/2^-$  states have been observed at  
 516 1711, 981, and 1010 keV, respectively [8], lying very close  
 517 to the  $7/2^-$  particle-core coupling states. While for the  
 518 latter, the  $B(E2; 7/2^- \rightarrow 3/2^-)$  values rapidly increase  
 519 from 4.6(7) W.u. in  $^{69}\text{Cu}$  to 14.9(18) W.u. in  $^{73}\text{Cu}$  [9],  
 520 low  $B(E2; 7/2^- \rightarrow 3/2^-)$  values ( $< 3$  W.u.) have been  
 521 measured in  $^{69,71}\text{Cu}$  for the  $7/2^-$  “intruder” states [10].  
 522 These intruder states have been associated with a  $1f_{7/2}^{-1}$   
 523 proton-hole configuration [54]. In  $^{69}\text{Cu}$ , the  $7/2^-$  state  
 524 at 1711 keV was found, in transfer reactions [40, 42], to  
 525 contain around one third of the  $\pi 1f_{7/2}^{-1}$  strength, with a  
 526  $C^2S$  about 5 times larger than that of the  $7/2^-$  particle-  
 527 core coupling state. However, a similar experiment per-  
 528 formed for  $^{71}\text{Cu}$  did not find any significant part of the  
 529  $\pi 1f_{7/2}^{-1}$  strength below 2 MeV, questioning the proton-  
 530 hole character of the 981 keV state. In  $^{69,71}\text{Cu}$ ,  $\Delta I = 1$   
 531 bands have been observed on top of the  $7/2^-$  intruder  
 532 states, using multi-nucleon transfer reactions [13–15]. In  
 533  $^{73}\text{Cu}$ , the state at 1489 keV was assigned  $9/2^-$  spin and  
 534 parity, and proposed to be a member of the  $\pi 1f_{7/2}^{-1}$  in-  
 535 truder band [8]. In  $^{77}\text{Cu}$ , the  $7/2^-$  intruder state at 2068  
 536 keV was first observed in the  $\beta$ -decay of  $^{77}\text{Ni}$  [7], and  
 537 the assignment was based on the results of the MCSM  
 538 calculations, which found the state to be dominated by  
 539 a seven proton occupancy in the  $\pi 1f_{7/2}$  orbital (74%).  
 540 This state was later strongly populated in the proton  
 541 knockout experiment of Ref. [16], supporting its  $1f_{7/2}^{-1}$   
 542 proton-hole character. In the proton knockout experi-  
 543 ment of Ref. [17], none of the populated states in  $^{79}\text{Cu}$   
 544 was identified to contain a large fraction of the  $\pi 1f_{7/2}^{-1}$   
 545 strength.

546 The systematics of the  $7/2^-$  intruder states in  $^{69-77}\text{Cu}$   
 547 and the band members up to spin  $11/2^-$  are shown  
 548 in Fig. 11a. In the present work, the excited states at  
 549 1484, 1989, and 2516 keV in  $^{75}\text{Cu}$  are assigned, respec-  
 550 tively,  $7/2^-$ ,  $9/2^-$  and  $11/2^-$  spins and parities, and are  
 551 proposed to be members of the  $\pi 1f_{7/2}^{-1}$  intruder band.  
 552 The assignment is based on the similarity of the obser-  
 553 ved decay sequence with the  $9/2^- \rightarrow 7/2^-$  and the  
 554  $11/2^- \rightarrow 9/2^-$  transitions in  $^{69-73}\text{Cu}$  and the compari-  
 555 son with the MCSM values (see Fig. 6). The proton-hole  
 556 character of the 1484 and 2068 keV states in  $^{75}\text{Cu}$  and  
 557  $^{77}\text{Cu}$ , respectively, has been now confirmed in the proton  
 558 knockout experiment of Ref [21].

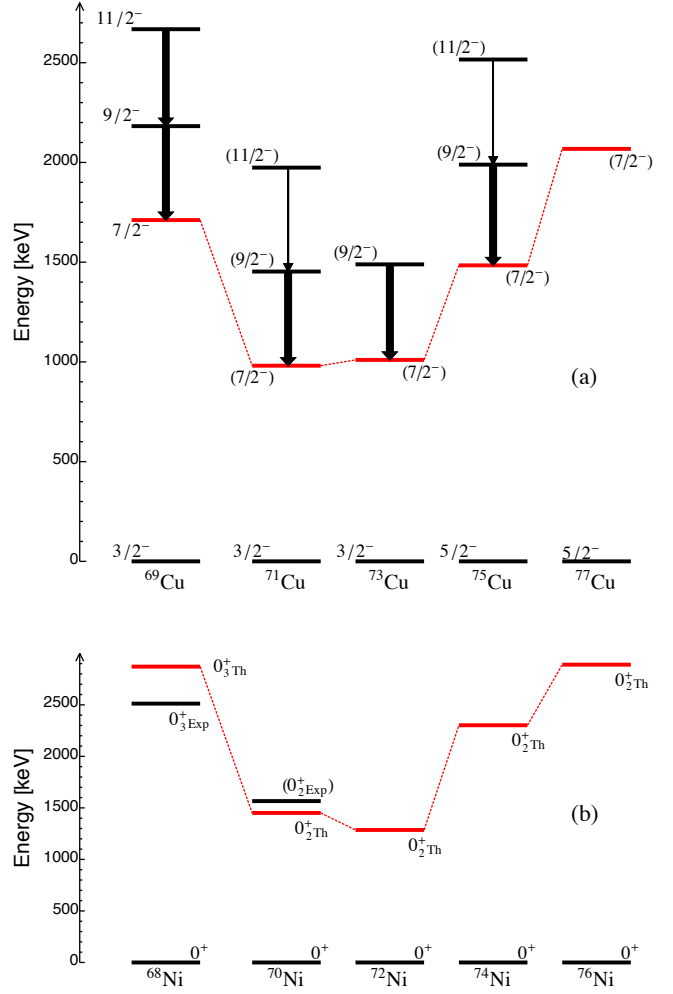


FIG. 11. (Color online) (a) Systematics of the intruder states in odd-A  $^{69-77}\text{Cu}$  isotopes. The widths of the  $11/2^- \rightarrow 9/2^-$  transitions in each isotope. The relative intensities were taken from the  $\beta$ -decay experiment of Ref. [8], except for  $^{69}\text{Cu}$ , where the  $11/2^-$  state has only been seen in Ref. [13]. (b) Intruder  $0^+$  states in the corresponding Ni cores. The experimental  $0_{\text{Exp}}^+$  states in  $^{68,70}\text{Ni}$  are those in Refs. [44, 46]. The MCSM values of the  $0_{\text{Th}}^+$  energies have been previously presented in Ref. [37].

559 The  $\pi 1f_{7/2}^{-1}$  intruder states in odd-mass Cu isotopes  
 560 with  $N \geq 40$ , have been suggested to be formed by the  
 561 coupling of one proton in the  $\pi 1f_{7/2}$  orbital to excited  
 562  $0^+$  states in the corresponding even-even Ni cores [15].  
 563 These excited  $0^+$  states are expected to have a prolate  
 564 shape, originated by the promotion of two protons from  
 565 the  $\pi 1f_{7/2}$  orbital across the  $Z = 28$  shell gap [37, 52]. In  
 566  $^{75}\text{Cu}$ , the MCSM calculations find the occupation num-  
 567 ber of the  $\pi 1f_{7/2}$  orbital to be 6.71 for the  $7/2_2^-$  in-  
 568 truder state, and similar values are found for the cor-  
 569 responding states in  $^{77}\text{Cu}$  and  $^{79}\text{Cu}$ : 6.68 and 6.82, re-  
 570 spectively. This state is found by the calculations to  
 571 be prolate, with an average deformation of  $\beta \sim 0.27$

(see Fig. 7). The collectivity of the intruder band is expected to be large; for  $^{77}\text{Cu}$ , the MCSM calculations find  $B(E2, 9/2^- \rightarrow 7/2^-) = 34$  W.u. The calculated energies of the prolate  $0^+$  states in the even-even  $^{68-76}\text{Ni}$  isotopes are shown in Fig. 11b. Candidates for these yrare  $0^+$  states and their  $2^+$  and  $4^+$  band members have been proposed in  $^{68}\text{Ni}$  [44, 45, 52, 55] and  $^{70}\text{Ni}$  [46, 47, 56]. In  $^{72}\text{Ni}$ , two states observed at 2010 and 2320 keV were suggested to be possible prolate intruder states [57], as well as in  $^{76}\text{Ni}$ , for an observed state at 2995 keV [51].

The MCSM calculations explain the presence of the prolate, deformed bands at relatively low energies at  $N \sim 42, 44$  as an effect of the Type II shell evolution [37, 38]. While the  $\nu 1g_{9/2}$  orbital is expected to follow a normal filling in the ground-state bands of the  $38 \leq N \leq 48$ , even-even Ni isotopes with a maximum of collectivity at  $N \sim 44, 46$  [53] (where the  $\nu 1g_{9/2}$  orbital can thus be expected to be half filled), the addition of two protons from the  $1f_{7/2}$  orbital to the  $pf$  shell favors the occurrences of  $\pi 1f_{5/2} - \nu 1g_{9/2}$  quadrupole correlations and precipitates the filling of the  $\nu 1g_{9/2}$  orbital in the intruder band, reaching half of the total occupancy at  $N \sim 42, 44$ . For Ni isotopes with  $N > 44$ , the Type II shell evolution is suppressed because of the increasing occupancy of the  $\nu 1g_{9/2}$  orbital, therefore, the deformation of the prolate band decreases and the energy of the prolate  $0^+$  state is expected to increase gradually from  $^{72}\text{Ni}$  to  $^{76}\text{Ni}$ . As can be seen in Fig. 11, the intruder states in odd-mass  $^{69-77}\text{Cu}$  isotopes follow a parabolic trend very similar to the predicted one for the yrare, prolate  $0^+$  states in the  $^{68-76}\text{Ni}$  isotopes. The asymmetry of the parabola can be understood as an effect of the Type I shell evolution [37, 38]: the energy of the  $7/2^-$  intruder state in  $^{75}\text{Cu}$  is lower than the energy of the corresponding  $7/2^-$  state in  $^{69}\text{Cu}$  because of reduction of the  $\pi 1f_{7/2} - \pi 1f_{5/2}$  single-particle gap under the influence of the monopole component of the nucleon-nucleon interaction [2, 3].

## V. SUMMARY AND CONCLUSIONS

Excited states in  $^{75}\text{Cu}$  up to  $\sim 4$  MeV were populated in the  $\beta$ -decay of  $^{75}\text{Ni}$ . The  $^{75}\text{Ni}$  nuclei were produced at the RIBF in RIKEN, in the in-flight fission of  $345A$  MeV  $^{238}\text{U}$  projectiles on a  $^9\text{Be}$  target. The fragments were selected and identified in the BigRIPS fragment separator and later implanted in a stack of DSSSDs for the detection of the  $\beta$ -decay electrons. The EURICA array

of HPGe cluster detectors was used for the detection of the  $\beta$ -delayed  $\gamma$ -rays. A level scheme was proposed based on the  $\gamma$ - $\gamma$  coincidence analysis, from which the location of the two previously known low-lying isomeric states was clarified. MCSM calculations were performed on the  $pf g_{9/2} d_{5/2}$  model space for both neutrons and protons, using the A3DA interaction. The level structure below 2 MeV was interpreted based on the results of the shell model calculations and the systematics of odd-A Cu isotopes with  $N \geq 40$  and their corresponding even-even Ni cores. Different single-particle, core-coupling, and intruder states were proposed, and spins and parities were assigned for these states. The remaining states shown in the level scheme of Fig. 5 are less straight forward to interpret and probably highly mixed in their wave functions. In the light of the new experimental information presented in this work, together with the recent results in  $^{77}\text{Cu}$  [7] and  $^{79}\text{Cu}$  [17], the evolution of the low-lying states in  $^{69-79}\text{Cu}$  was discussed.

## ACKNOWLEDGMENTS

This work was carried out at the RIBF operated by RIKEN Nishina Center, RIKEN and CNS, University of Tokyo. The research leading to the results has received funding from the Research Council of Norway under project Grants No. 240104 and No. 213442 and from KAKENHI (under Grants No. 25247045, No. 23.01752, and No. 25800130); U.S. DOE Grant No. DE-FG02-91ER-40609; Spanish Ministerio de Ciencia e Innovación Contracts No. FPA2009-13377C02 and No. FPA2011-29854-C04; and the Hungarian Scientific Research Fund OTKA Contract No. K100835. The Monte Carlo shell model calculations were performed on K computer at RIKEN AICS (hp140210, hp150224, hp160211). This work was supported in part by the HPCI Strategic Program (The Origin of Matter and the Universe), by "Priority Issue on Post-K computer" (Elucidation of the Fundamental Laws and Evolution of the Universe) (hp160211), and by CNS-RIKEN joint project for large-scale nuclear structure calculations. The authors acknowledge the EUROBALL Owners Committee for the loan of germanium detectors and the PreSpec Collaboration for the readout electronics of the cluster detectors. Part of the WAS3ABi has been supported by the Rare Isotope Science Project which is funded by the Ministry of Education, Science and Technology (MEST) and National Research Foundation (NRF) of Korea.

- 
- [1] O. Sorlin and M.-G. Porquet, Prog. Part. Nucl. Phys. **61**, 602 (2008).  
 [2] T. Otsuka *et al.*, Phys. Rev. Lett. **104**, 012501 (2010).  
 [3] T. Otsuka, Phys. Scr. T **152**, 014007 (2013).  
 [4] K. Sieja and F. Nowacki, Phys. Rev. C **81**, 061303(R) (2010).  
 [5] K. T. Flanagan *et al.*, Phys. Rev. Lett. **103**, 142501 (2009).  
 [6] U. Köster *et al.*, Phys. Rev. C **84**, 034320 (2011).  
 [7] E. Sahin *et al.*, Phys. Rev. Lett. **118**, 242502 (2017).  
 [8] S. Franchoo *et al.*, Phys. Rev. C **64**, 054308 (2001).  
 [9] I. Stefanescu *et al.*, Phys. Rev. Lett. **100**, 112502 (2008).

- 676 [10] E. Sahin *et al.*, Phys. Rev. C **91**, 034302 (2015).  
677 [11] R. Grzywacz *et al.*, Phys. Rev. Lett. **81**, 766 (1998).  
678 [12] T. Ishii *et al.*, Phys. Rev. Lett. **81**, 4100 (1998).  
679 [13] T. Ishii *et al.*, Phys. Rev. Lett. **84**, 39 (2000).  
680 [14] I. Stefanescu *et al.*, Phys. Rev. C **79**, 034319 (2009).  
681 [15] S. N. Liddick *et al.*, Phys. Rev. C **92**, 024319 (2015).  
682 [16] Zs. Vajta *et al.*, Phys. Lett. B **782**, 99 (2018).  
683 [17] L. Olivier *et al.*, Phys. Rev. Lett. **119**, 192501 (2017).  
684 [18] J. M. Daugas *et al.*, Phys. Rev. C **81**, 034304 (2010).  
685 [19] C. Petrone *et al.*, Phys. Rev. C **94**, 024319 (2016).  
686 [20] Y. Ichikawa *et al.*, Nature Physics **15**, 321 (2019).  
687 [21] E. Sahin *et al.*, to be submitted.  
688 [22] P.-A. Söderström *et al.*, Nucl. Instr. Meth B **317**, 649-652  
689 (2013).  
690 [23] T. Motobayashi, H. Sakurai, Prog. Theor. Exp. Phys.  
691 **2012**, 03C001.  
692 [24] H. Okuno, N. Fukunishi, and O. Kamigaito  
693 Prog. Theor. Exp. Phys. **2012**, 03C002.  
694 [25] T. Kubo *et al.*, Prog. Theor. Exp. Phys. **2012**, 03C003.  
695 [26] J. P. Dufour *et al.*, Nucl. Instr. Meth A **248**, 267 (1986).  
696 [27] Z. Y. Xu, Ph.D. thesis, Department of Physics, Univer-  
697 sity of Tokyo (2014). <http://hdl.handle.net/2261/57714>  
698 [28] N. Fukuda *et al.*, Nucl. Instr. Meth. B **317**, 323-332  
699 (2013).  
700 [29] Z. Y. Xu *et al.*, Phys. Rev. Lett. **113**, 032505 (2014).  
701 [30] S. Nishimura, Prog. Theor. Exp. Phys. **2012**, 03C006.  
702 [31] P. Hosmer *et al.*, Phys. Rev. C **82**, 025806 (2010).  
703 [32] The Evaluated Nuclear Structure Data File, ENSDF.  
704 <http://www.nndc.bnl.gov/ensdf/>  
705 [33] Brlcc, Conversion Coefficient Calculator.  
706 <http://bricc.anu.edu.au>
- 707 [34] M. Wang *et al.*, Chin. Phys. C, 1603 (2012).  
708 [35] C. J. Chiara *et al.*, Phys. Rev. C **85**, 024309 (2012).  
709 [36] T. Otsuka *et al.*, Phys. Rev. Lett. **95**, 232502 (2005).  
710 [37] Y. Tsunoda *et al.*, Phys. Rev. C **89**, 031301(R) (2014).  
711 [38] T. Otsuka and Y. Tsunoda, J. Phys. G: Nucl. Part. Phys.  
712 **43**, 024009 (2016).  
713 [39] N. Shimizu *et al.*, Prog. Theor. Exp. Phys. 01A205  
714 (2012).  
715 [40] B. Zeidman and J. A. Nolen, Phys. Rev. C **18**, 2122  
716 (1978).  
717 [41] F. Ajzenberg-Selove *et al.*, Phys. Rev. C **24**, 1762 (1981).  
718 [42] P. Morfouace *et al.*, Phys. Rev. C **93**, 064308 (2016).  
719 [43] P. Morfouace *et al.*, Phys. Lett. B **751**, 306 (2015).  
720 [44] F. Recchia *et al.*, Phys. Rev. C **88**, 041302(R) (2013).  
721 [45] F. Flavigny *et al.*, Phys. Rev. C **91**, 034310 (2015).  
722 [46] C. J. Prokop *et al.*, Phys. Rev. C **92**, 061302(R) (2015).  
723 [47] A. I. Morales *et al.*, Phys. Lett. B **765**, 328 (2017).  
724 [48] A. I. Morales *et al.*, Phys. Rev. C **93**, 034328 (2016).  
725 [49] C. Mazzocchi *et al.*, Phys. Lett. B **662**, 45 (2005).  
726 [50] T. Marchi *et al.*, Phys. Rev. Lett. **113**, 182501 (2014).  
727 [51] P.-A. Söderström *et al.*, Phys. Rev. C **92**, 051305(R)  
728 (2015).  
729 [52] S. Suchyta *et al.*, Phys. Rev. C **89**, 021301(R) (2014).  
730 [53] K. Kolos *et al.*, Phys. Rev. Lett. **116**, 122502 (2016).  
731 [54] A. M. Oros-Peusquens and P. F. Mantica, Nucl. Phys. A  
732 **669**, 81 (2000).  
733 [55] D. Pauwels *et al.*, Phys. Rev. C **82**, 027304 (2010).  
734 [56] C. J. Chiara *et al.*, Phys. Rev. C **91**, 044309 (2015).  
735 [57] W. B. Walters *et al.*, AIP Conference Proceedings **1681**,  
736 030007 (2015).